Available online at www.sciencedirect.com
ScienceDirect
Materials Chemistry and Physics 103 (2007) 407–414
MATERIALS CHEMISTRY AND PHYSICS
www.elsevier.com/locate/matchemphys

The influence of Fe_2O_3 in the humidity sensor performance of ZrO_2:TiO_2-based porous ceramics

I.C. Cosentino, E.N.S. Muccillo, R. Muccillo *

Centro Multidisciplinar de Desenvolvimento de Materiais Cerâmicos, CCTM, Instituto de Pesquisas Energéticas e Nucleares, C.P. 11049, S. Paulo 05422-970, SP, Brazil

Received 1 August 2005; received in revised form 27 April 2006; accepted 18 February 2007

Abstract

ZrO_2:TiO_2 ceramics were prepared with different porosity values by two methods: (a) sintering at 1150, 1300 and 1500 °C, corresponding to the temperatures of the first, second and third sintering stages, according to dilatometry results; (b) adding Fe_2O_3 (2.0 and 5.0 mol%) to ZrO_2:TiO_2 powders before sintering. The ZrO_2:TiO_2 specimens were characterized by X-ray diffraction, mercury porosimetry, scanning electron microscopy and impedance spectroscopy. The impedance spectroscopy analysis was carried out under different relative humidities. The bulk electrical resistivity in the low frequency region (10–100 Hz) decreases for increasing relative humidity. Increasing the sintering temperature from the first to the third sintering stage promoted grain growth, as expected, with consequent decrease of the intergranular porosity. The use of Fe_2O_3 as sintering aid reduced the porosity of the specimens, but increased the electrical response under humid environments in comparison with specimens sintered without Fe_2O_3.

Keywords: Chemical synthesis; Porous ceramics; Zirconium titanate

1. Introduction

The mechanisms to explain the electrical response of ceramic materials to humidity take into account the chemically and physically adsorbed layers of water molecules as well as the capillary condensation of water inside tiny pores. The porous microstructure and the surface reactivity with water are key parameters for the performance of ceramic humidity sensors [1]. Ceramics with large pore volume, suitable pore size distribution and large surface area usually have high sensitivity to humidity [2,3]. Water is adsorbed when porous ceramics are exposed to humidity, leading to an increase of their electrical conductivity [2,4–6]. The sensitivity of the ceramic humidity sensors depends on the microstructure, which is related with the process of ceramics fabrication.

Humidity sensors are increasingly being required for humidity monitoring in a series of industrial processes. Several ceramic materials have been proposed to be used in humidity sensing devices. The main advantages of ceramic sensing devices are better mechanical, chemical and thermal stability, wide range of operation temperature and fast response to humidity change [7,8]. Porous ceramics like $MgCr_2O_4$–TiO_2, $MgAl_2O_4$, Al_2O_3, SiO_2, TiO_2 and $BaSrTiO_3$ [9], SnO_2 [10], proton conducting perovskite ceramics [11,12], yttria-stabilized zirconia [13], and ZnO [14] have been proposed as ceramic sensor component in humidity sensing devices. The presence of a large pore volume with a suitable pore size distribution is considered fundamental to achieve a high sensitivity to humidity [15]. The electrical impedance of the ceramic decreases for increasing humidity due to the increase of the physically adsorbed water and also to the condensation of water in capillars [16]. In the low humidity range, the mechanism is known as the Grottus chain reaction. In this case, the charge transport occurs via proton release by H_3O^+ to a neighbor water molecule, which, by its turn, releases another proton starting a chain reaction. For high humidity environments there is water condensation in the pores, giving rise to an electrolytic conduction along with the proton conduction at the adsorbed layers [15]. The humidity sensitivity is strongly correlated to the microstructure of the porous ceramic. Therefore, average pore size, pore distribution and specific surface area are key parameters for specifying the properties of a ceramic to be used in humidity sensing devices. The actual number of

* Corresponding author. Tel.: +55 1138169343; fax: +55 1138169343.
E-mail address: ceramica@ipen.br (R. Muccillo).

0254-0584/$ – see front matter © 2007 Elsevier B.V. All rights reserved.
doi:10.1016/j.matchemphys.2007.02.051

sites for water molecule adsorption is also important and can be increased by changing the defect structure of the porous ceramic lattice [16].

We report here the results on preparation and properties of zirconia–titania (ZrO_2:TiO_2) ceramics with different pore volume distributions by sintering cold-pressed specimens at different temperatures. Some specimens were also prepared using Fe_2O_3 as sintering modifier to obtain specimens with different porosities. All specimens had their electrical behavior studied by impedance spectroscopy at room temperature under different relative humidities. X-ray diffraction, mercury porosimetry, scanning electron microscopy and impedance spectroscopy were the main techniques for the analysis of structural phases, pore volume distribution, bulk morphology and electrical response, respectively.

2. Experimental

Ceramic ZrO_2:TiO_2 powders were prepared according to the polymeric precursor technique described elsewhere [17]. Additions of Fe_2O_3 (2.0 and 5.0 mol%) to the ZrO_2:TiO_2 powders were done for modifying the microstructure of sintered pellets. Iron carbonate (Alfa Aesar) was mixed to the ZrO_2:TiO_2 powders before sintering. The degree of stoichiometry of the ZrO_2:TiO_2 powder was analyzed by X-ray fluorescence in a Jordan Valley ED-XRF model Ex-Calibur spectrometer. Powders prepared by the polymeric precursor technique had 50.1% Ti and 49.9% Zr. The powders were pressed to 10 mm diameter and 1 mm thickness cylindrical pellets. The linear shrinkage was measured in a Netzsch DIL 402/E/7 dilatometer at 10 °C min^{-1} heating rate with a 2 h holding time at 1600 °C. The temperatures 1150, 1300 and 1500 °C were then chosen as the sintering temperatures for obtaining specimens with different pore densities. The pore size distribution in the 0.03–360 μm range was evaluated by mercury porosimetry in a Micromeritics Autopore III porosimeter.

X-ray diffraction of the sintered pellets was measured at room temperature in the 25–40° 2θ range using a Bruker-AXS D8 Advance X-ray diffractometer, with a θ–2θ Bragg–Brentano configuration, operating at 40 kV–40 mA with Cu Kα radiation and scintillation detector.

Scanning electron microscopy analysis of fracture surfaces of sintered ZrO_2:TiO_2 specimens was carried out in a model 440I LEO microscope.

For impedance spectroscopy measurements, silver electrodes were applied by coating the parallel surfaces of the sintered specimens with colloidal silver and curing at 350 °C 30 min^{-1}. The impedance spectroscopy measurements were carried out at room temperature in a 4192A Hewlett Packard Impedance Analyzer connected to a series 362 HP Controller for collecting the $[-Z''(\omega) \times Z'(\omega)]$ impedance data via a HPIB interface. The range of the frequency ($\omega/2\pi$) was 5 Hz–13 MHz and the signal amplitude 100 mV. The software developed by M. Kleitz (LIESG, Grenoble, France) was used to control the impedance analyzer and to collect data [18]. Cylindrical specimens were placed inside a sample chamber specially designed for electrical measurements under different humidity conditions. The sample chamber consists of a glass chamber with a lucite lid and stainless steel feed-thru electrodes, designed to keep the samples in a constant humidity environment. The relative humidity (RH), the ratio of actual vapor pressure to the saturated vapor pressure at a given temperature, was the parameter used to specify humidity. The humidity was kept constant at room temperature in the 29–84% relative humidity range using standard saturated solutions of $CaCl_2 \cdot 6H_2O$, $Mg(NO_3)_2$, NH_4NO_3, NH_4Cl and KCl salts. The relative humidity RH values were determined according to the equation RH (%) = $A \exp(B/T)$, A and B are constants that depend on the temperature for each salt [19] and T is the absolute temperature. The temperature of the specimens was monitored with a chromel–alumel thermocouple with its sensing tip located close to the specimens.

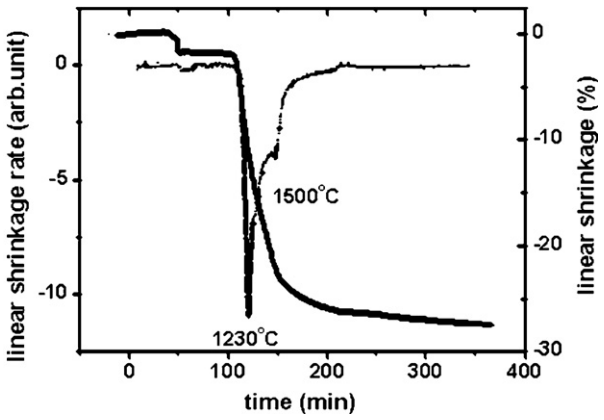

Fig. 1. Linear shrinkage as a function of heating time for ZrO_2:TiO_2 ceramic green pellets. Heating rate: 10 °C min^{-1}; maximum temperature 1600 °C.

3. Results and discussion

The sequence for describing the results is the following: dilatometric data for choosing suitable temperatures for specific degrees of porosity, X-ray diffraction data for structural phase characterization, pore size distribution data for characterizing pore network, scanning electron microscopy for morphology observations, and impedance spectroscopy data for electrical behavior under different relative humidities.

Fig. 1 shows the linear shrinkage behavior of ZrO_2:TiO_2 cold pressed powders, in the range room temperature −1600 °C, for a heating rate of 10 °C min^{-1}. The time derivative of the linear shrinkage is also shown. Two temperatures are indicated: 1230 and 1500 °C. The former corresponds to the maximum linear shrinkage rate, which is caused by elimination of small pores (see Fig. 3) and to volume reduction due to a decrease of the b-axis value (1100–1200 °C range) corre-

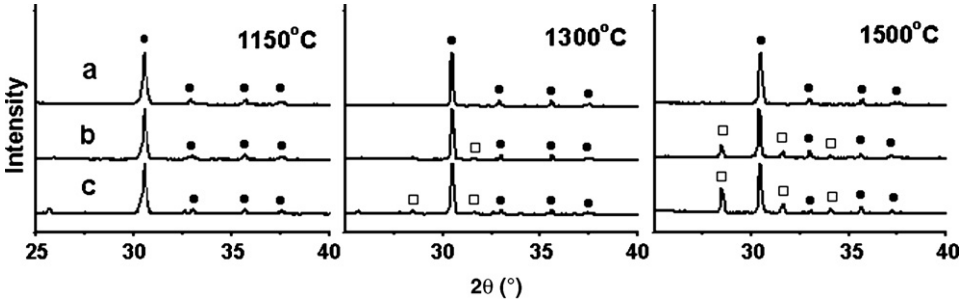

Fig. 2. X-ray diffraction patterns of ZrO_2:TiO_2 + x mol% Fe_2O_3 ceramic pellets sintered at 1150, 1300 and 1500 °C. (●) $ZrTiO_4$ and (□) monoclinic ZrO_2; (a) (x = 0), (b) (x = 2.0), (c) (x = 5.0).

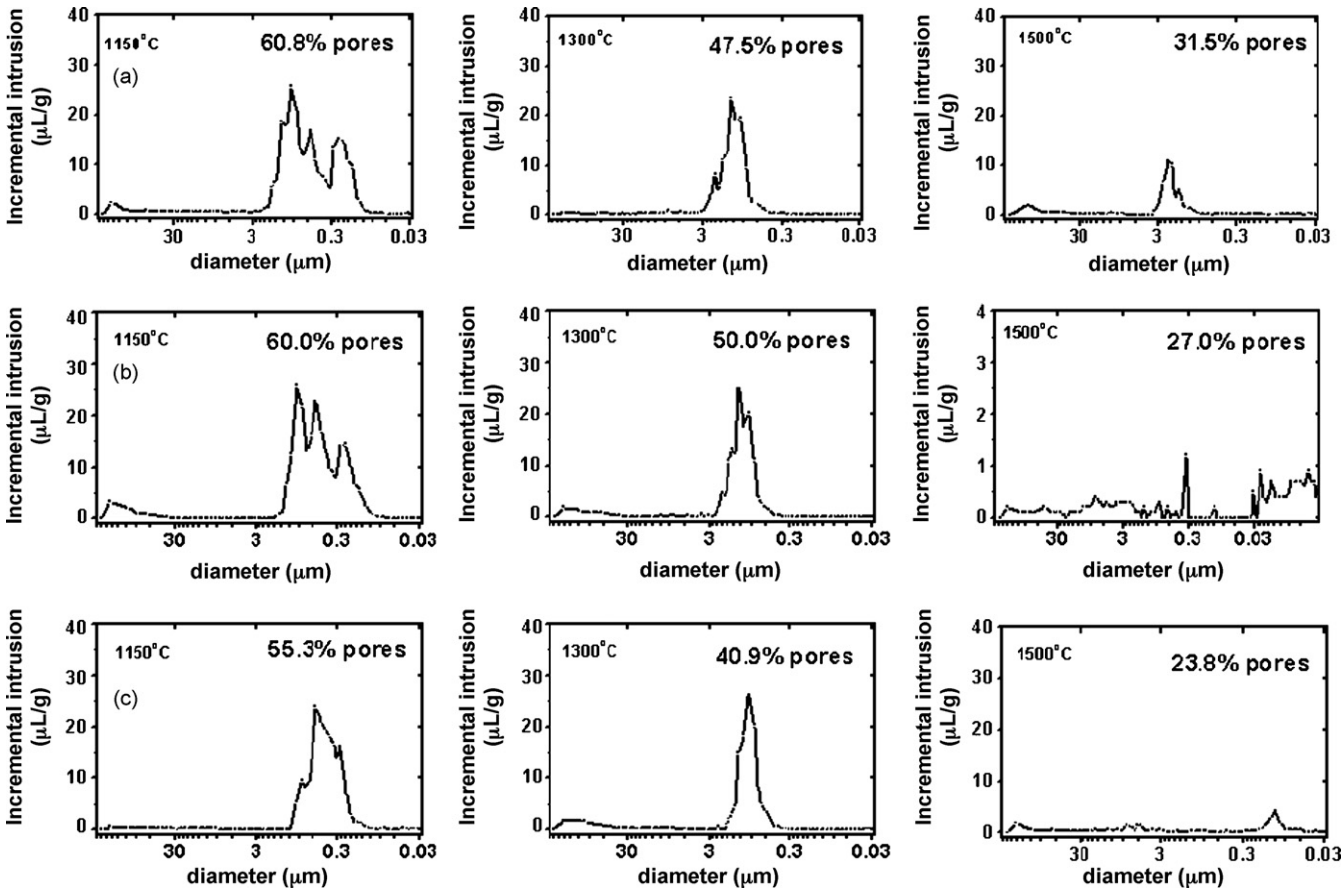

Fig. 3. Incremental intrusion as a function of pore diameter of ZrO_2:TiO_2 + x mol % Fe_2O_3 (x = 0, 2.0, 5.0) ceramic pellets sintered at 1150, 1300 and 1500 °C; (a) (x = 0), (b) (x = 2.0), (c) (x = 5.0).

sponding to an order–disorder transition in the orthorhombic structure [20]. The latter corresponds to a second maximum linear shrinkage rate due to elimination of large pores (see Fig. 3). For temperatures higher than 1500 °C, the grain growth phenomenon is predominant. According to these results, 1150, 1300 and 1500 °C were chosen as the temperatures for sintering ZrO_2:TiO_2 in order to obtain ceramic specimens with different porosities.

Fig. 2 shows results of X-ray diffraction analysis of flat surfaces of ZrO_2:TiO_2 pellets sintered at 1150, 1300 and 1500 °C, without Fe_2O_3 (a) and with 2.0 mol% (b) and 5.0 mol% (c) of Fe_2O_3. According to the ICDD file #80-1783, only the orthorhombic $ZrTiO_4$ phase is present in samples sintered at 1150 °C. Similarly, specimens sintered at 1300 and 1500 °C without Fe_2O_3 addition are also single phase orthorhombic $ZrTiO_4$. The addition of Fe_2O_3 leads to the formation of the monoclinic ZrO_2 phase, evidenced by the (−1 1 1) and (1 1 1) reflections at 2θ equal to 28.11° and 31.6°, respectively (ICDD file #37-1484). Their intensities increase for increasing Fe_2O_3 content and sintering temperature.

The results of mercury porosimetry of all ZrO_2:TiO_2 specimens are shown in Fig. 3. From left to right, increasing the temperature decreases the pore volume due to sintering, as expected. From top to bottom, increasing the Fe_2O_3 content decreases the pore volume because Fe_2O_3 might be acting as sintering aid via a liquid phase sintering mechanism [21]. Moreover, the addition of Fe_2O_3 may change the average pore size and the pore size distribution, as shown for specimens without and with 5% Fe_2O_3 sintered at 1500 °C.

The dependence of the open porosity content on the sintering temperature of ZrO_2:TiO_2, sintered with addition of Fe_2O_3 is shown in Fig. 4. The behavior is similar for samples sintered at 1150 °C and at 1300 °C without Fe_2O_3 and with 2.0 mol% Fe_2O_3: increasing the sintering temperature to 1500 °C promotes a large decrease in open porosity; the

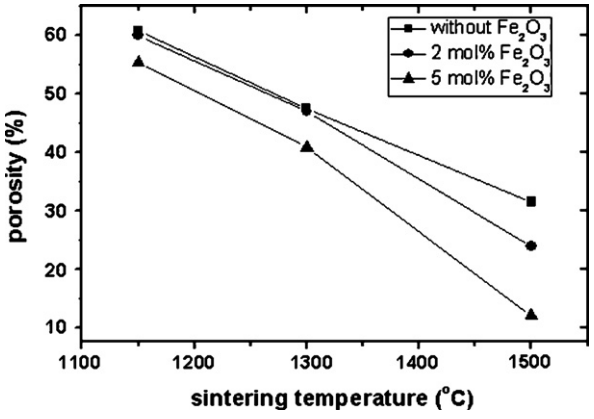

Fig. 4. Dependence of the open porosity on the sintering temperature of ZrO_2:TiO_2 ceramic pellets with different Fe_2O_3 content.

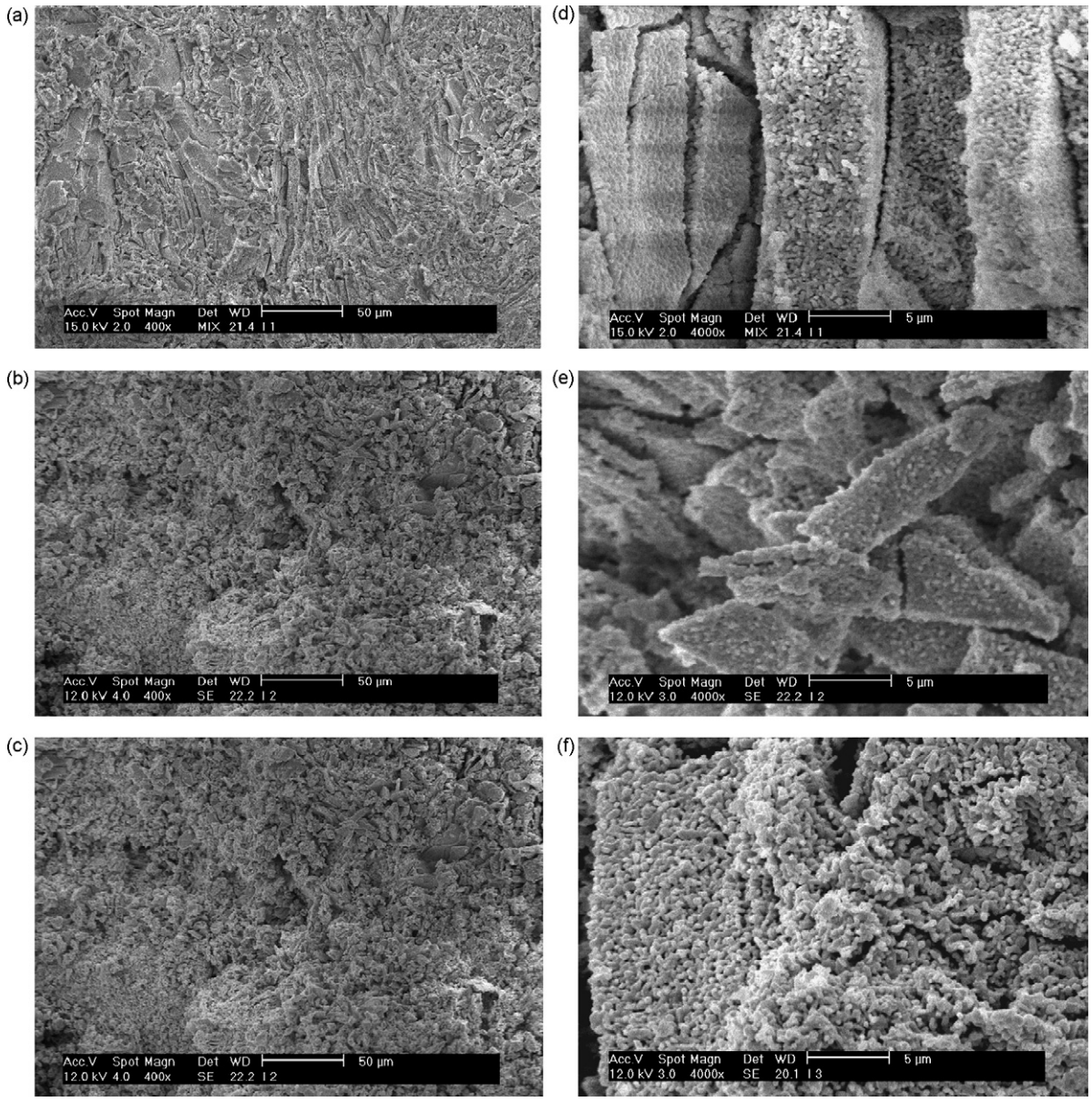

Fig. 5. Scanning electron microscopy micrographs of fractured surfaces of ZrO_2:TiO_2 ceramic pellets with different Fe_2O_3 additions: without Fe_2O_3 (a and d); with 2.0 mol% Fe_2O_3 (b and e); with 5.0 mol% Fe_2O_3 (c and f). The figures on the right are higher magnification of the figures on the left.

main effect of the addition of Fe_2O_3 is to inhibit the formation of pores. The addition of 5.0 mol % Fe_2O_3 to ZrO_2:TiO_2 sintered at 1500 °C promotes a decrease from 30% to 12% pore content. Sintering at high temperatures and adding Fe_2O_3 are suggested as suitable procedures for preparing porous specimens.

3.1. Effect of Fe_2O_3 content on the microstructure and electrical properties

Fig. 5 shows typical results of scanning electron microscopy analysis of fracture surfaces of ZrO_2:TiO_2 sintered at 1150 °C. A preliminary observation shows that all compositions contain submicron particles consisting of dense agglomerates.

The agglomerates of samples sintered without Fe_2O_3 addition may be described as elongated plates. The addition of 2.0 mol% Fe_2O_3 results on reduction of the agglomerate average size and also on the aspect ratio. The addition of 5.0 mol% Fe_2O_3 produces sintered ceramics with higher densities. After the structural and microstructural characterizations, silver electrodes were applied to the sintered ZrO_2:TiO_2 pellets for electrical characterization.

Fig. 6 shows $[-Z''(\omega) \times Z'(\omega)]$ impedance spectroscopy diagrams of ZrO_2:TiO_2 without and with Fe_2O_3 addition (2.0 and 5.0 mol%) sintered at 1500 °C. All measurements were carried out at room temperature under different humidity conditions. One semicircle may be resolved at the high frequency region of the impedance diagrams, corresponding to the electrical response of the bulk porous ceramics. The higher is the relative humidity in the sample cell the lower is the electrical resistivity of the specimens (determined by the intercept of the fitted semicircle with the x axis towards the low frequency region).

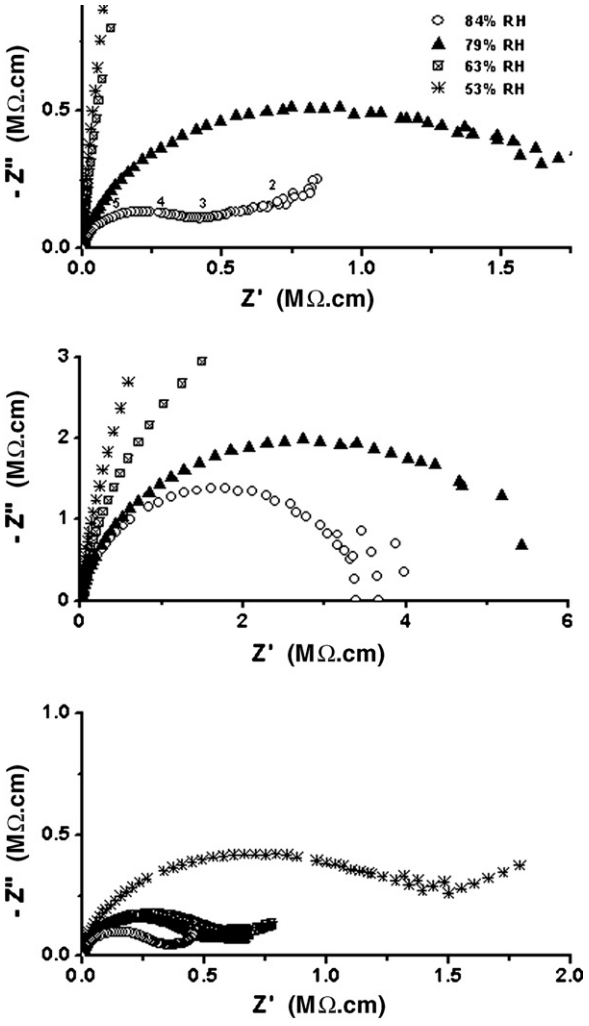

Fig. 6. Impedance spectroscopy diagrams of ZrO_2:TiO_2 + x mol% Fe_2O_3, $x = 0$ (top), 2.0 (middle) and 5.0 (bottom) ceramic pellets, measured under different relative humidities.

This is expected because the number of available charge carriers increases when the humidity is higher. It has already been reported that the physical adsorption and capillarity condensation of water molecules at the internal surfaces of the porous ceramic specimens promote an increase of the charge carrier concentration with a decrease of the electrical resistivity [22]. Here it was also found that the use of Fe_2O_3 as sintering aid helps reducing further the electrical resistivity of samples, comparing with samples without Fe_2O_3 sintered at the same temperature. Two might be the reasons for this behavior: the pore morphology and the substitution of Fe^{3+} ions for Zr^{4+} and/or Ti^{4+} ions, increasing the catalytic action of the internal surfaces under reaction with water species.

Fig. 7 shows the dependence of Z', the real component of the impedance on the frequency of the applied signal. These values were obtained at room temperature under four different relative humidities inside the sample cell. In the 10–100 Hz range Z' does not depend on the frequency, but only on the relative humidity. This is an indication that simple two-probe low frequency ac measurements could be applied for the study of the dependence

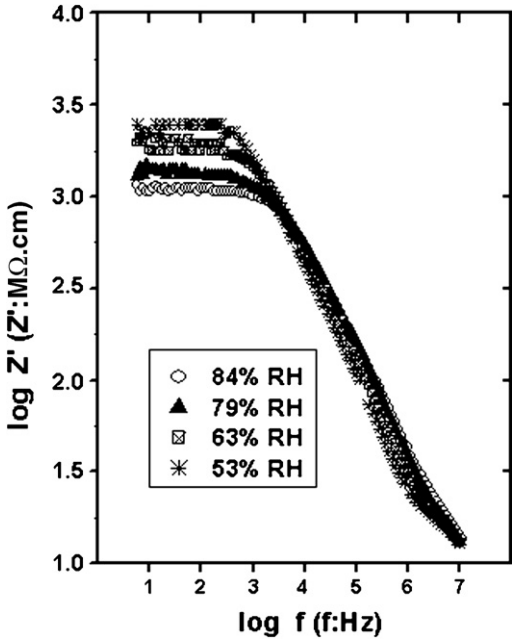

Fig. 7. Dependence of the electrical resistivity on the frequency for ZrO_2:TiO_2 ceramic pellets under different relative humidities.

of the electrical resistance on the humidity and, consequently, porous ZrO_2:TiO_2 may be considered as good candidate for humidity sensing devices [23].

Fig. 8 shows ac electrical resistivity values of ZrO_2:TiO_2 porous ceramics measured at 100 Hz, as a function of the relative humidity. The resistance values were considered at 100 Hz because they belong to the semicircle responsible for the detection of water species and are far from data scattering due to electrode polarization at lower frequencies. The addition of

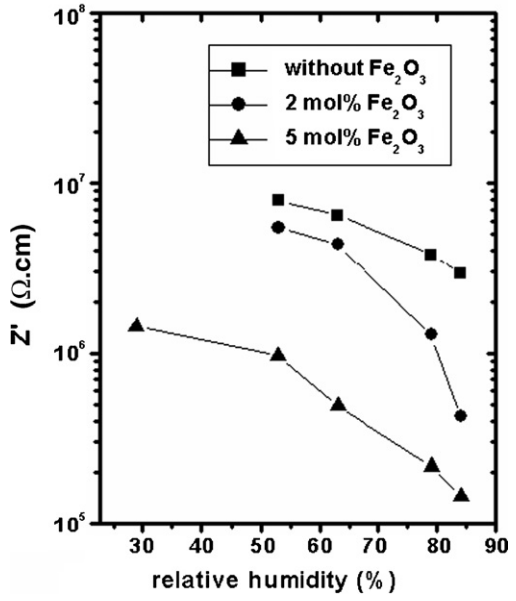

Fig. 8. Dependence of the electrical resistivity on the relative humidity. Values measured at 100 Hz in ZrO_2:TiO_2 + x mol% Fe_2O_3 ($x = 0$, 2.0, 5.0) ceramic pellets sintered at 1500 °C.

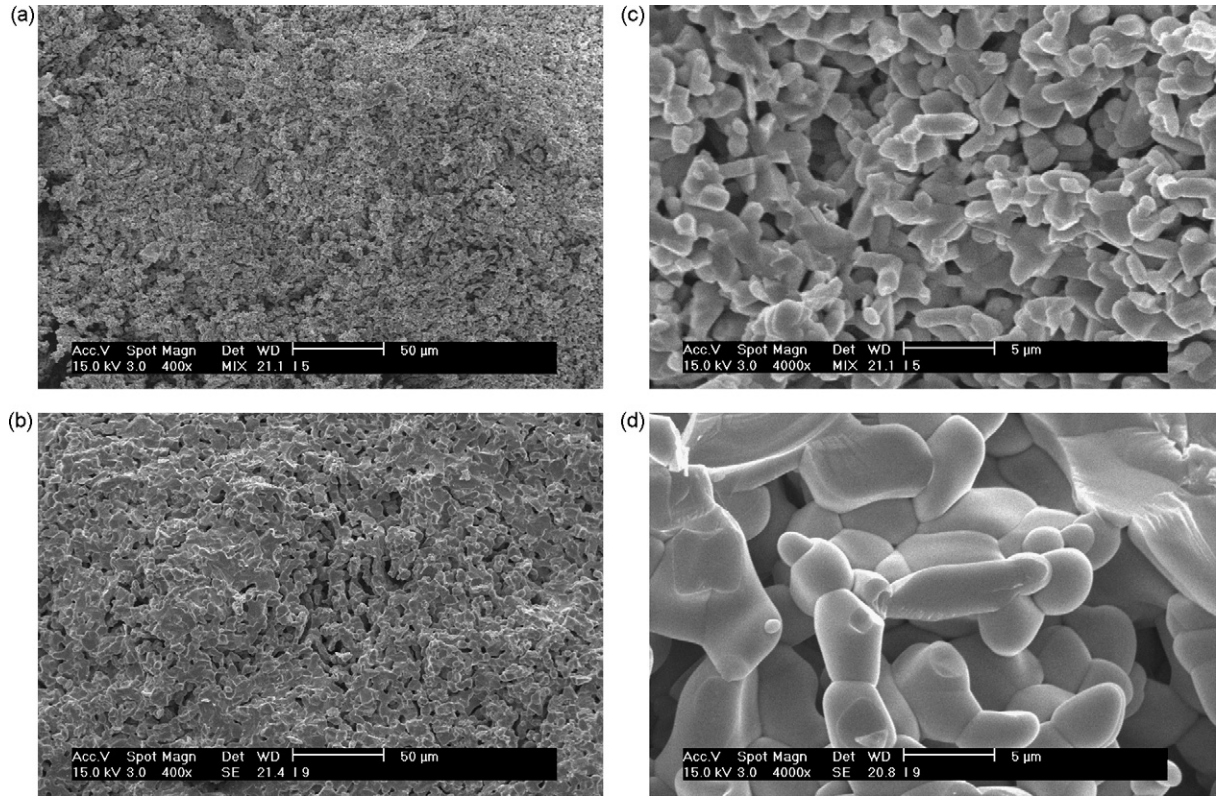

Fig. 9. Scanning electron microscopy micrographs of fractured surfaces of ZrO_2:TiO_2 ceramic pellets sintered at 1300 °C (a and c), and 1500 °C (b and d). The figures on the right are higher magnification of the figures on the left.

Fe_2O_3 to ZrO_2:TiO_2 causes a decrease of the electrical resistivity for the same relative humidity conditions. This is probably due to the increase in the number of adsorption sites of ZrO_2:TiO_2 sintered with Fe_2O_3 addition [24]. Water adsorption in the internal surfaces of the porous ceramics is important for the electrical conduction, being dominant for low relative humidity. The larger is the specific surface area, the larger is the content of adsorbed water and, consequently, the larger is the density of charge carriers, usually mobile protons [25]. The values of specific surface area determined by the BET method are presented in Table 1. Increasing the Fe_2O_3 content results in increasing specific surface area.

The ZrO_2:TiO_2 porous ceramic pellet sintered with 2.0 mol% Fe_2O_3 addition shows higher sensitivity to water than the one with 5.0 mol% addition. This is probably related to the mesopore volume, which is the main responsible for the amount of condensed water in a porous ceramic [19]. Indeed, our results on mercury porosimetry show that the ZrO_2:TiO_2 pellets with 2.0 mol% Fe_2O_3 addition have the largest volume of mesopores.

Table 1
Values of specific surface area of ZrO_2:TiO_2 + x mol% Fe_2O_3 (x = 0, 2.0 and 5.0) ceramic powders

Composition	Specific surface area ($m^2\ g^{-1}$)
ZrO_2:TiO_2	37.1 ± 0.1
ZrO_2:TiO_2 + 2.0 mol% Fe_2O_3	43.8 ± 0.2
ZrO_2:TiO_2 + 5.0 mol% Fe_2O	45.5 ± 0.2

3.2. Effect of the sintering temperature on the microstructure and electrical properties

Fig. 9 shows typical results of scanning electron microscopy analysis of fracture surfaces of ZrO_2:TiO_2 pellets sintered at 1300 and 1500 °C without Fe_2O_3 addition. According to Fig. 5a, the ceramic pellet sintered at 1150 °C shows large dense agglomerates of submicron size particles, with high pore volume (~61%). The increase of the sintering temperature to 1300 °C (Fig. 9a and c) promotes grain growth, neck formation between grains and the decrease of porosity to ~47%. The pellets sintered at 1500 °C (Fig. 9b and d), on the other hand, show even larger grain growth and grain coalescence. Moreover, the microstructure becomes denser with a pore volume of ~31%.

Fig. 10 shows $[-Z''(\omega) \times Z'(\omega)]$ impedance diagrams of ZrO_2:TiO_2 pellets sintered at 1150, 1300 and 1500 °C, measured at room temperature under different relative humidity conditions. Only one well defined semicircle is observed. As shown before (cf. Fig. 6), increasing the relative humidity reduces the electrical resistivity of the ZrO_2:TiO_2 pellets. The effect of the sintering temperature is also shown: ceramic pellets sintered at 1300 °C shows the lower values of electrical resistivity. The main reason may be found in the microstructure (cf. Figs. 5 and 9). At 1150 °C the microstructure is not homogeneous and the agglomerates have a platelet-like shape. At 1300 °C sintering is achieved, the grains are small and there are interconnected pores (paths for electrical conduction). At 1500 °C the grains are

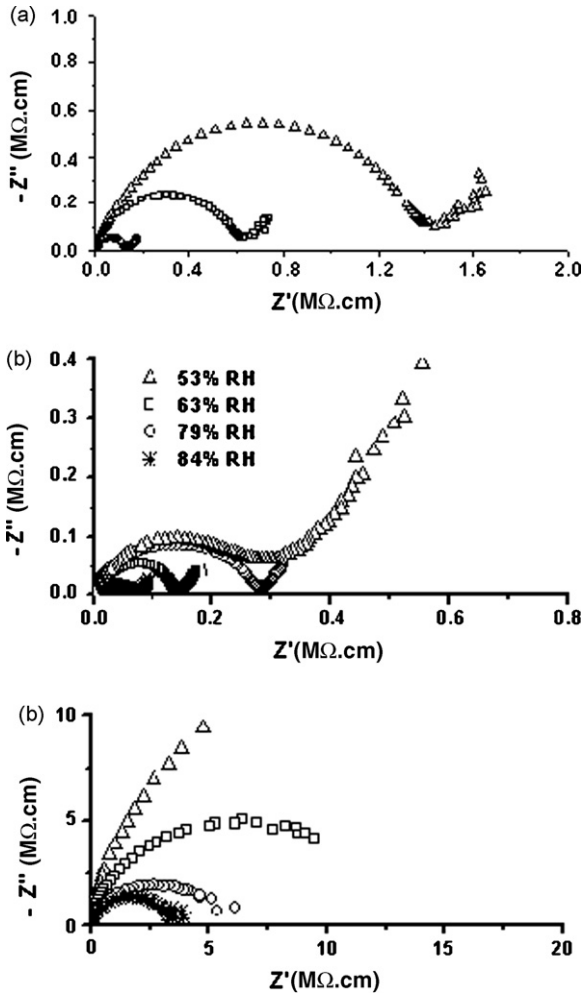

Fig. 10. Impedance spectroscopy diagrams of ZrO_2:TiO_2 ceramic pellets sintered at 1150 °C (a), 1300 °C (b) and 1500 °C (c), measured at different relative humidities.

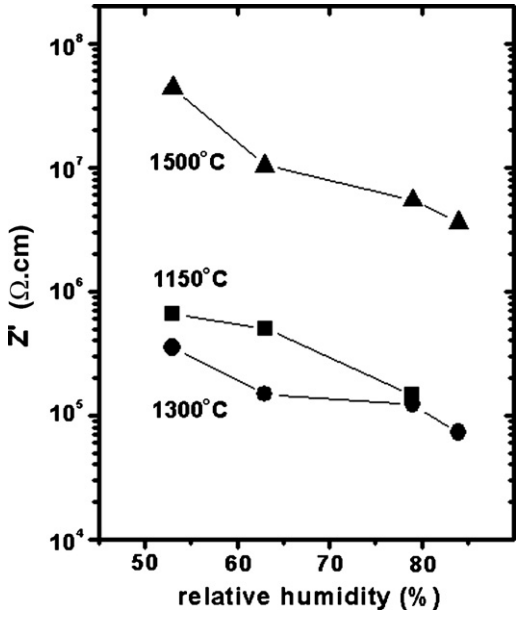

Fig. 11. Values of electrical resistivity, measured at 100 Hz under different humidity conditions, of ZrO_2:TiO_2 ceramic pellets sintered at 1150, 1300 and 1500 °C.

larger that at 1300 °C and the density of interconnected pores is lower.

Fig. 11 shows the effect of the sintering temperature on the electrical properties of ZrO_2:TiO_2 porous ceramics. The resistivity of ZrO_2:TiO_2 sintered at 1500 °C is higher than those of specimens sintered at lower temperatures for all RH conditions due to its denser microstructure. The specimens sintered at 1300 °C present the lower values of electrical resistivity. Increasing the sintering temperature from 1150 to 1300 °C causes the disappearance of pores with average diameter approximately 2 μm, which do not contribute to water condensation [19].

4. Conclusions

ZrO_2:TiO_2 ceramic powders were prepared by the polymeric precursor technique. Ceramic pellets prepared with these powders show electrical resistivity behavior dependent on the relative humidity. The addition of Fe_2O_3 results in a reduction of the electrical resistivity. The increase of the sintering temperature promoted grain growth and reduction of both pore volume and pore average size. ZrO_2:TiO_2 specimens sintered at 1300 °C show the lowest value of electrical resistivity at room temperature, being promising candidates for room temperature humidity sensing devices.

Acknowledgements

To CNEN, FAPESP (99/10798-0 and 98/14324-0), CNPq (RM: Proc. 306496/88, ENSM: Proc. 300934/94-7) and PRONEX for financial support. To Y.V. França for thermal analysis and to I. Sayeg (Instituto de Geociências, USP) for SEM analysis.

References

[1] G. Fu, H. Chen, Z. Chen, J. Zhang, H. Kohler, Sens. Actuators B 81 (2002) 308.
[2] Y. Shimizu, H. Arai, T. Seiyama, Sens. Actuators 7 (1985) 11.
[3] T.Y. Kim, D.H. Lee, Y.C. Shim, J.U. Bu, S.T. Kim, Sens. Actuators B 9 (1992) 221.
[4] J.H. Anderson, G.A. Parks, J. Phys. Chem. 72 (1968) 3362.
[5] E. McCafferty, A.C. Zettlemoyer, Disc. Faraday Soc. 52 (1971) 239.
[6] E. Traversa, Sens. Actuators B 23 (1995) 135.
[7] N. Yamazoe, Y. Shimizu, Sens. Actuators 10 (1986) 379.
[8] T.J. Hwang, G.M. Choi, J. Am. Ceram. Soc. 76 (1993) 766.
[9] J. Wang, Feng-Qing Wu, Kai-He Shi, Xiao-Hua Wang, Peng-Po Sun, Sens. Actuators B 99 (2004) 586.
[10] I. Skuratovsky, A. Glot, E. Di Bartolomeo, E. Traversa, R. Polini, J. Eur. Ceram. Soc. 24 (9) (2004) 2597.
[11] W. Wang, A.N. Virkar, Sens. Actuators B 98 (2–3) (2004) 282.
[12] T. Schober, Solid State Ionics 162 (2003) 277.
[13] M. Nakatou, N. Miura, Electrochem. Commun. 6 (10) (2004) 995.
[14] Y. Zhang, K. Yu, D. Jiang, Z. Zhu, H. Geng, L. Luo, Appl. Surf. Sci. 242 (1–2) (2005) 212.
[15] F. Fabregat-Santiago, N.S. Ferriols, G. Garcia-Belmonte, Appl. Phys. Lett. 80 (2002) 2785.
[16] Y. Shimizu, H. Okada, H. Arai, J. Am. Ceram. Soc. 72 (1989) 436.
[17] I.C. Cosentino, E.N.S. Muccillo, R. Muccillo, Sens. Actuators B 96 (2003) 677.

[18] M. Kleitz, J.H. Kennedy, in: P. Vashishta, J.N. Mundy, G.K. Shenoy (Eds.), Fast Ion Transport in Solids, North Holland, The Netherlands, 1979, p. p185.
[19] D.R. Lide (Ed.), Handbook of Chemistry and Physics, 75th ed., CRC Press, Florida, 1994, pp. 15–25.
[20] P. Bordet, A. McHale, A. Santoro, R.S. Roth, J. Solid State Chem. 64 (1986) 30.
[21] R.M. German, Sintering Theory and Practice, Wiley Interscience, N. York, 1966.
[22] M. Pelino, C. Cantalini, H.-T. Sun, M. Faccio, Sens. Actuators B 46 (1998) 186.
[23] M. Greenblatt, P. Shuk, Solid State Ionics 86–88 (1996) 995.
[24] M.K. Jain, M.C. Bhatnagar, G.L. Sharma, Jpn. J. Appl. Phys. 39 (2000) 345.
[25] Kan-Sen Chou, Tzy-Kuang Lee, Feng-Jün Liu, Sens. Actuators B 56 (1999) 106.